Computer Vision and Image Understanding 235 (2023) 103776

Contents lists available at ScienceDirect

Computer Vision and Image Understanding

journal homepage: www.elsevier.com/locate/cviu

Addressing multiple salient object detection via dual-space long-range dependencies

Bowen Deng, Andrew P. French, Michael P. Pound *

Computer Vision Laboratory, School of Computer Science, University of Nottingham, United Kingdom

ARTICLE INFO

Communicated by Nikos Paragios

MSC:
41A05
41A10
65D05
65D17

Keywords:
Salient object detection
Attention
Dual-space long-range dependencies
Non-local neural networks

ABSTRACT

Salient object detection plays an important role in many downstream tasks. However, complex real-world scenes with varying scales and numbers of salient objects still pose a challenge. In this paper, we directly address the problem of detecting multiple salient objects across complex scenes. We propose a network architecture incorporating non-local feature information in both the spatial and channel spaces, capturing the long-range dependencies between separate objects. Traditional bottom-up and non-local features are combined with edge features within a feature fusion gate that progressively refines the salient object prediction in the decoder. We show that our approach accurately locates multiple salient regions even in complex scenarios. To demonstrate the efficacy of our approach to the multiple salient objects problem, we curate a new dataset containing only multiple salient objects. Our experiments demonstrate the proposed method presents state-of-the-art results on five widely used datasets without any pre-processing and post-processing. We obtain a further performance improvement against competing techniques on our multi-objects dataset. The dataset and source code are available at: https://github.com/EricDengbowen/DSLRDNet.

1. Introduction

Salient object detection (SOD) aims to highlight the most visually striking or important objects of a scene. SOD plays a significant role in computer vision pipelines, and has been widely applied to many object-level applications in various areas such as object recognition (Rutishauser et al., 2004), object detection (Ren et al., 2013; Zhang et al., 2017), image retrieval (He et al., 2012), image captioning (Das et al., 2017; Fang et al., 2015), weekly supervised semantic segmentation (Wang et al., 2018c; Wei et al., 2016) and image cropping (Wang et al., 2018a).

Although remarkable progress has been made, there still remain many open challenges. Existing SOD datasets contain many images with a single object, often centered in the middle of the image. Human observers may be drawn naturally to centered objects, but in complex scenes they can identify numerous salient objects distributed throughout a scene. Many existing techniques in saliency are based upon traditional U-shape networks, containing only convolutional operations that process local neighborhoods. This fails to exploit the long-range pixel-wise or channel-wise relationships among features in an image, and ultimately leaves techniques less able to address the problem of multiple salient objects (Fig. 1). Long-range dependencies have been shown to play an important role in different classification tasks (Wang et al., 2018b), and this is also true of pixel-level segmentation works such as salient object detection. The size of the receptive field is significant in locating and segmenting salient objects across the image. Large kernels aid segmentation tasks but the experimental receptive fields are usually smaller than the ones in theory (Liu et al., 2019; Zhao et al., 2017; Peng et al., 2017). This will likely limit the performance of SOD networks in which objects are spatially separated.

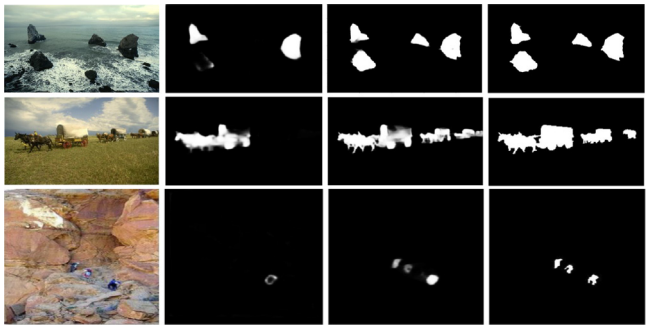

Fig. 1. Visual examples of our proposed method. After introducing dual-space long-range dependencies, our model can handle complicated scenes with multiple salient objects.

* Corresponding author.
E-mail address: michael.pound@nottingham.ac.uk (M.P. Pound).

https://doi.org/10.1016/j.cviu.2023.103776
Received 8 November 2021; Received in revised form 14 June 2023; Accepted 4 July 2023
Available online 8 July 2023

Recent state-of-the-art SOD approaches solve the problem of salient object detection in the general case, often by combining and refining multi-level features into feature representations (Hou et al., 2017; Zhang et al., 2018a; Wu et al., 2019a,b; Zhao et al., 2019; Liu et al., 2019), introducing additional losses into frameworks to provide structural information (Feng et al., 2019; Qin et al., 2019) or applying attention mechanisms to filter the redundant information and focus on the valuable features (Zhang et al., 2018b; Liu et al., 2018; Chen et al., 2018; Feng et al., 2019; Wu et al., 2019a). Only few of the existing SOD methods consider long-range dependencies (Liu et al., 2020; Li et al., 2020; Zhou et al., 2020; Sun et al., 2019), and none of these works specifically address the problem of multiple salient objects.

In this paper, we propose a novel architecture for multiple salient object detection that considers long-range dependencies in both spatial space and channel space. Inspired by Fu et al. (2019) and Wang et al. (2018b), we propose a non-local guidance module (NLGM), comprising several dual-space non-local blocks (DSNLBs) to capture pixel-wise and channel-wise relationships. Features at each position are aggregated by a weighted sum of all the features in spatial space, while each channel map is updated by a weighted integration of all interdependent channel maps. Unlike previous work, we stack several DSNLBs in order to capture non-local features in a progressive manner. Bottom-up convolutional features and these non-local features are combined in the network decoder through feature fusion gates, that control the transmission of information into the next stage of the network. These include salient edge supervision to further enhance the quality of the saliency maps. We demonstrate the improved performance of our network on numerous datasets, and specifically multiple salient object detection (MSOD) problems by evaluating on a dataset containing only complex multi-saliency images. Our contributions are:

- We propose a novel MSOD framework that models long-range dependencies in both spatial space and channel space. To the best of our knowledge, this is the first paper that explicitly models long-range dependencies in this dual space for standard SOD and MSOD problems.
- We utilize non-local guidance and edge refinement modules that work complementarily to enrich feature representations at each stage of the top-down pathway. Features from all components are combined within a feature fusion gate, which utilizes edge features to promote relevant salient and non-local features. The fusion gate ensures that top-down features are passed discriminatively through the network.
- We curate a new dataset containing only multiple salient objects, drawn from popular datasets in this field. We compare the proposed approach against 14 state-of-the-art methods on five widely used SOD benchmarks and the proposed multi-object dataset. Without any pre-processing and post-processing, our proposed method exceeds all previous state-of-the-art approaches in three evaluation metrics and provides a further performance boost against competing techniques on our proposed dataset.

2. Related work

Traditional salient object detection methods mostly rely on low-level features (Zhu et al., 2014; Jiang et al., 2013) or heuristic priors such as color contrast (Cheng et al., 2014) and background (Wei et al., 2012; Yang et al., 2013). More details are introduced in the survey by Borji et al. (2019).

Early deep SOD methods utilized multi-scale image patches (Li and Yu, 2015; Wang et al., 2015; Zhao et al., 2015), offering impressive performance, but limited by the lack of spatial information found in small image patches. Since the introduction of fully convolutional networks (FCNs) (Long et al., 2015), there have been many effective and efficient end-to-end SOD architectures. Among these, U-shape based architectures (Ronneberger et al., 2015) see much use. Hou et al. (2019, 2017) applied short connections from deeper to shallower layers, integrating high-level and low-level features. Zhang et al. (2018a) used a gated pathway for bi-directional message passing and multi-level feature integration. Zhang et al. (2018b) embedded multi-path recurrent connections and spatial attention modules to generate saliency maps. Chen et al. (2018) designed a reverse attention block to emphasize non-object areas. Qin et al. (2019) applied another bottom-up/top-down architecture to refine the coarse saliency map generated from the prediction network. This work generates boundary-aware saliency maps through a hybrid loss approach. Feng et al. (2019) employed global perceptron modules and attentive feedback modules to detect global saliency and build encoder–decoder communication respectively. Zhao et al. (2019) explicitly modeled edge features to guide the multi-scale features extracted from a U-shape structure and then fused multiple side-outputs into a final saliency map. Liu et al. (2019) mainly investigated the role of pooling layer in U-shape structure. They proposed a global guidance module for transmitting localization information to top-down pathway and a feature aggregation module to further refine fused features. Wu et al. (2019b) introduced a cross refinement unit to exchange mutual information between edge features and saliency features. Zhao et al. (2020) designed a gated dual branch network incorporating a Fold-ASPP to better localize the salient objects of various scales. Pang et al. (2020) proposed a transformation–interaction–fusion strategy to obtain efficient multi-scale features and a consistency-enhanced loss to deal with the imbalance issue between foreground and background.

Existing SOD methods seldom consider long-range dependencies: the sharing of information across spatially distant pixels, or between feature maps in channel space. Of those that do, Li et al. (2020) and Sun et al. (2019) applied self-attention mechanisms to capture spatial long-range context. Zhou et al. (2020) introduced a multi-type self-attention to capture pixel-level relationships for saliency detection in degraded images. Liu et al. (2020) designed a self-mutual attention to capture long-range contextual dependencies, this time in RGB-D. Of these works, none have made use of channel-wise dependencies as we do here and there is no ideal solution for multiple salient object detection. This has previously been hard to examine; existing public datasets contain some multi-object instances, but the frequency of these varies substantially. Here we curate a dataset specifically for this purpose, allowing us to focus on this problem.

3. Proposed method

The architecture of our proposed method is shown in Fig. 2. Our model is based on a U-shape FCN combining a bottom-up pathway (backbone) and a top-down pathway. Similar to most deep SOD models, we use VGG network to illustrate our proposed structure. Following EGNet (Zhao et al., 2019) and DSS (Hou et al., 2017, 2019), the last three fully connected layers are truncated and an additional side path is connected to the last pooling layer of VGG. This provides 6 outputs from bottom-up pathway representing the multi-level features captured from Conv1-2 to Conv6-3, which can be defined as a feature set $S = \{S^1, S^2, S^3, S^4, S^5, S^6\}$.

Multi-scale saliency features are processed through the top-down pathway with a series of convolutional blocks, each containing 3 convolutional layers and ReLU activations. We refer to this saliency feature set as $F = \{F^1, F^2, F^3, F^4, F^5, F^6\}$, where F^6 is the saliency feature produced by the sixth convolutional block (rightmost Conv in Fig. 2) and so on.

We leverage intermediate supervision (Lee et al., 2015) at each convolutional block to improve training performance. For each saliency feature F^i, a convolutional layer D^i_F is applied to produce a single-channel prediction. We use a cross-entropy loss, with the supervision

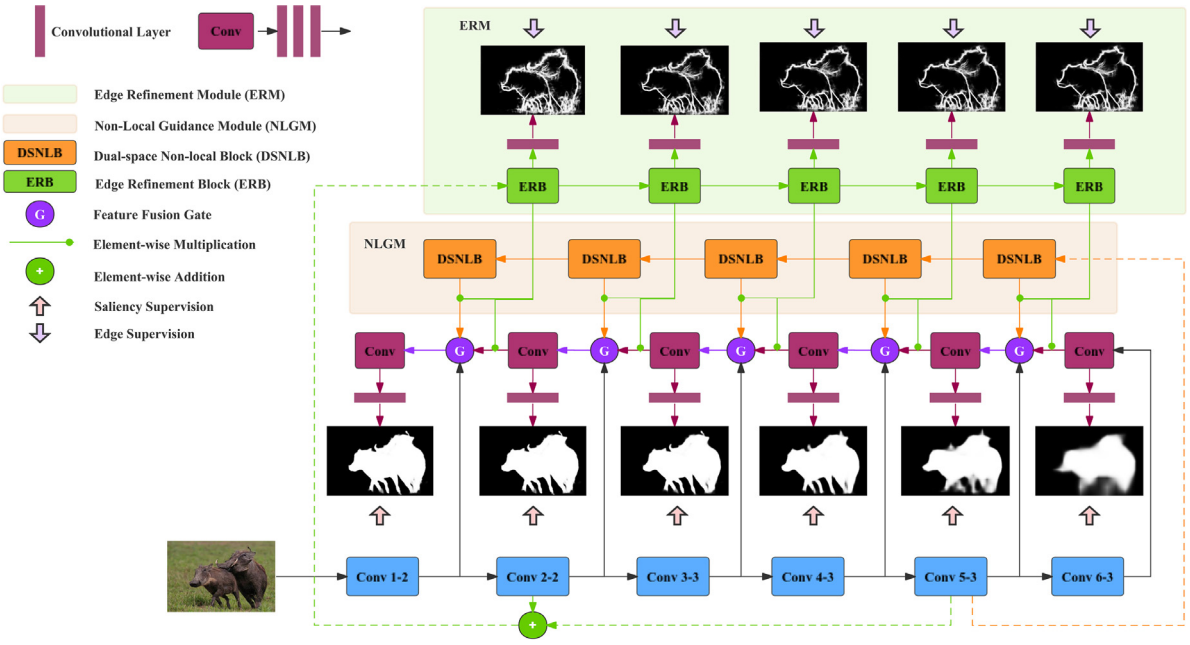

Fig. 2. The overall pipeline of our proposed approach, here shown using a VGG backbone. The red, orange and green boxes capture saliency features, non-local features and edge features respectively. Element-wise multiplication operates between each pair of ERB-DSNLB (edge and non-local features) and ERB-Conv (edge and saliency features). Our final prediction map is generated based on the fusion of 6 multi-scale saliency features in top-down pathway. (For interpretation of the references to color in this figure legend, the reader is referred to the web version of this article.)

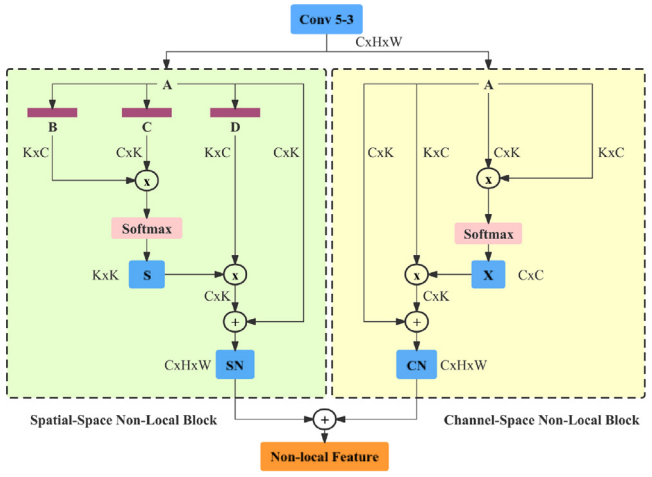

Fig. 3. The architecture of a dual-space non-local block (DSNLB). C, H and W demonstrate the channel number, height and width of given feature map respectively and $K = H \times W$.

here defined as:

$$\mathcal{L}_F^i\left(F^i, W_{DF}^i\right) = -\sum_{j\in Y^+} \log Pred\left(y_j = 1|F^i; W_{DF}^i\right) - \sum_{j\in Y^-} \log Pred\left(y_j = 0|F^i; W_{DF}^i\right), i \in [1,6], \quad (1)$$

where Y^+ and Y^- denote the pixels in salient region and non-salient region respectively. W_{DF}^i denotes the parameters of convolutional layer D_F^i. $Pred\left(y_j = 1|F^i; W_{DF}^i\right)$ denotes the salient prediction map.

3.1. Non-local guidance module

In this module we model long-range dependencies in both spatial and channel space. Inspired by Fu et al. (2019), we make use of dual-space non-local information within two parallel pathways that capture pixel-wise contextual information and channel-wise relationships. Unlike (Fu et al., 2019), which directly append a single attention module on top of FCN for scene segmentation, our NLGM is composed of 5 stacked dual-space non-local blocks (DSNLBs), one at each stage of the top-down pathway. We choose the feature map S^5 extracted from Conv5-3 as the input of the NLGM as it contains high-level semantic information, and yet contains more spatial information than S^6. Fig. 3 illustrates the detailed structure of the first DSNLB.

3.1.1. Spatial-space non-local block

For a given feature map $\mathbf{A} \in \mathbb{R}^{C\times H\times W}$, 3 convolutional layers are used to generate 3 distinct feature maps $\{\mathbf{B}, \mathbf{C}, \mathbf{D}\} \in \mathbb{R}^{C\times H\times W}$, representing query, key and value respectively. $\mathbf{B}$, $\mathbf{C}$ and $\mathbf{D}$ are reshaped to $\mathbb{R}^{C\times K}$, where $K = H \times W$. A unified similarity matrix $\mathbf{S} \in \mathbb{R}^{K\times K}$ is calculated as:

$$\mathbf{S} = f(\mathbf{B}^{\mathrm{T}} \times \mathbf{C}). \quad (2)$$

We apply a $softmax$ normalization function for f here. The weight matrix $\mathbf{S}$ models the affinity of features between any two spatial positions. The final weighted feature map SN in spatial space can be defined as:

$$SN = (\mathbf{S}^{\mathrm{T}} \times \mathbf{D})^{\mathrm{T}} + \mathbf{A}, \quad (3)$$

where $SN \in \mathbb{R}^{C\times H\times W}$ after reshaping. Informally, SN may be thought of as an enriched feature representation with global spatial perception, as each value of SN is a selective weighted sum of all positions across the whole feature map.

3.1.2. Channel-space non-local block

Given same feature map $\mathbf{A} \in \mathbb{R}^{C\times H\times W}$, reshaped to $\mathbb{R}^{C\times K}$, the unified similarity matrix $\mathbf{X} \in \mathbb{R}^{C\times C}$ in channel space is calculated as:

$$\mathbf{X} = f(\mathbf{A} \times \mathbf{A}^{\mathrm{T}}), \quad (4)$$

where f indicates $softmax$ function and $\mathbf{X}$ measures the correlation between any two channels. The weighted feature map CN in channel space can be defined as:

$$CN = (\mathbf{X}^{\mathrm{T}} \times \mathbf{A}) + \mathbf{A}, \quad (5)$$

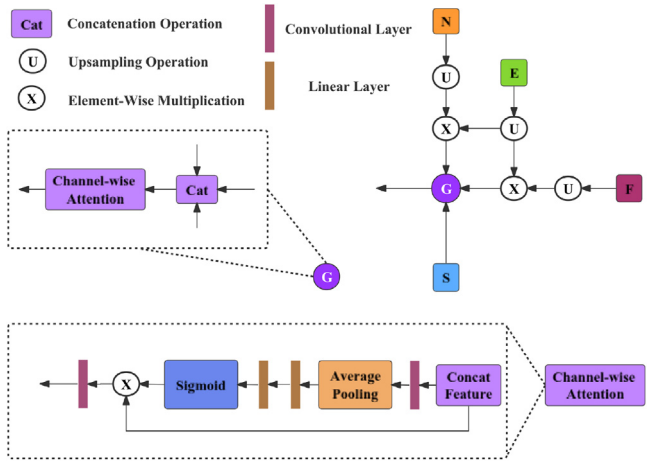

Fig. 4. The structure of a feature fusion gate. N, E, F and S demonstrate non-local feature, edge feature, saliency feature and the corresponding side output of bottom-up pathway respectively.

where $CN \in \mathbb{R}^{C\times H\times W}$ is a feature representation containing long-range dependencies within channel space. We do not make use of convolutional filters at the beginning of the channel-space non-local block. We hope to preserve the information in each channel without further filtering in order to directly calculate their relationships, similar to Fu et al. (2019).

3.1.3. Non-local feature aggregation

We combine the above features SN and CN to generate our non-local feature representations N, exploiting long-range contextual information in both spatial and channel space. N is given as:

$$N = D_N(SN + CN), \tag{6}$$

where D_N is a 1×1 convolutional layer.

3.1.4. Multi-hop communications

Our NLGM is composed of 5 DSNLBs, each generating non-local features N^i at each stage of top-down pathway. By stacking several DSNLBs, non-local features are progressively refined through multi-hop communication between features that share affinity both channel-wise and spatially. Relevant saliency-specific semantic information is shared across the image space and feature space. Since non-local features have a global view, the challenge of complex scenes and multiple salient objects are better addressed through this improved receptive field.

3.2. Feature fusion

The majority of the existing SOD models fuse different features without distinction. Redundant and mutually incompatible features from different objectives may harm overall performance once combined. As presented in Fig. 4, we leverage channel-wise attention to selectively aggregate different features at each stage of top-down pathway.

3.2.1. Edge refinement module

Motivated by the commonly used boundary detection in SOD models (Qin et al., 2019; Zhao et al., 2019), salient edge features are modeled, as part of the feature fusion gate, to support the training of non-local and salient features. Edge features are generated from low-level features S^2 and high-level features S^5 through bottom-up process, which are progressively refined within an Edge Refinement Module (ERM). We found that S^2 and S^5 outperformed S^1 and S^6 in this role. S^1 is lower level with a reduced receptive field size, while S^6 is high level, but has limited resolution.

The Edge Refinement Module (ERM) consists of 5 edge refinement blocks (ERBs) aligned with the respective blocks in the NLGM. Each ERB contains a convolutional layer followed by a ReLU function to generate salient edge features E^i at each stage. As with the salient features, we apply intermediate supervision in the ERM via a cross-entropy loss. A convolutional layer D_E^i is used to convert the edge feature to single-channel prediction map. The supervision here can be defined as:

$$\begin{aligned}\mathcal{L}_E^i\left(E^i, W_{DE}^i\right) = &-\sum_{j\in V^+}\log Pred\left(y_j = 1|E^i; W_{DE}^i\right)\\ &-\sum_{j\in V^-}\log Pred\left(y_j = 0|E^i; W_{DE}^i\right), i \in [1,5],\end{aligned} \tag{7}$$

where V^+ and V^- denote the set of salient edge pixels and other pixels respectively. W_{DE} indicates the parameters of D_E^i. We weight the two components of the above loss by the number of pixels in each class.

3.2.2. Feature fusion gate

Salient edge features are combined with salient and non-local features separately through element-wise multiplication. This operation serves to emphasize activations that are shared between feature maps, promoting complimentarity between the non-local, saliency and edge features. Features that are aligned between modules will train more quickly, with activations of those that are less relevant to other blocks reduced. The resulting salient and non-local features are then combined using channel-wise attention. Firstly, we unify the spatial size and channel count:

$$\hat{N}^i = Up(\delta(O(N^i;\theta)); S^i), i \in [1,5], \tag{8}$$

$$\hat{F}^i = Up(\delta(O(F^i;\theta)); S^{i+1}), i \in [2,6], \tag{9}$$

$$\hat{E}^i = Up(\delta(O(E^i;\theta)); S^i), i \in [1,5], \tag{10}$$

where $Up(*; S^i)$ upsamples $*$ to be the same size as S^i. $O(*;\theta)$ denotes a convolutional layer with parameter θ and δ is a ReLU activation function, which converts the channel number of $*$ to the channel number of S^i. The fused features F_{fusion}^i, including the incorporation of salient edge features, are calculated as:

$$F_{fusion}^i = CA(Cat(S^i, \hat{N}^i \otimes \hat{E}^i, \hat{F}^{i+1} \otimes \hat{E}^i)), \tag{11}$$

where $\otimes$ denotes the element-wise multiplication. Cat is the concatenation operation. CA indicates the channel-wise attention, which can be defined as:

$$CA(*, \theta_{ca}) = * \cdot (\sigma(fc_2(\delta(fc_1(ap(*, \theta_1))), \theta_2))), \tag{12}$$

where θ_{ca} denotes the parameters in channel-wise attention, ap is a global average pooling layer and fc is a fully-connected layer. σ and δ refer to the sigmoid function and ReLU functions respectively. The feature fusion gate here provides a mechanism to select the most useful channels for saliency from each module, fusing features with distinction (see Fig. 5).

3.3. Saliency inference

To make full use of the multi-scale saliency features, we hierarchically generate the final prediction map based on the fusion of six saliency features F^i from coarse-to-fine manner. This multi-scale fusion strategy also serves to reduce the risk of missing salient objects across multi-saliency visual scenes. Complementary features F^2, F^3, F^4, F^5, F^6 are upsampled and convolved to have equal spatial and feature size to F^1, they are then combined using element-wise addition to produce a final feature F_{fin}. A convolutional layer D_P is used to convert the feature map F_{fin} to a single-channel prediction map, trained using cross

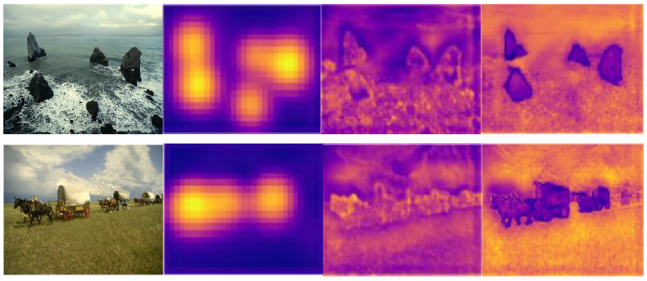

Fig. 5. Feature visualization of non-local features, edge features and the refined features after feature fusion. As can be seen, our non-local features highlight objects across the scene. After the feature fusion, multiple salient objects are clearly defined.

entropy:

$$\mathcal{L}_{fin}\left(F_{fin}, W_P\right) = -\sum_{j\in Y^+} \log Pred\left(y_j = 1|F_{fin}; W_P\right) - \sum_{j\in Y^-} \log Pred\left(y_j = 0|F_{fin}; W_P\right), \quad (13)$$

where Y^+ and Y^- denote the set of salient pixels and non-salient pixels respectively. W_P refers to the parameters of convolutional layer D_P. Therefore the total loss $\mathbb{L}$ in our proposed method can be denoted as:

$$\mathbb{L} = \sum_{i=1}^{6} \mathcal{L}_F^i(F^i; W_{DF}^i) + \sum_{i=1}^{5} \mathcal{L}_E^i(E^i; W_{DE}^i) + \mathcal{L}_{fin}\left(F_{fin}, W_P\right) \quad (14)$$

4. Experiments

4.1. Datasets

To demonstrate the performance of our proposed method, we evaluate our model on five widely used benchmark datasets: DUT-OMRON (Yang et al., 2013), HKU-IS (Li and Yu, 2015), DUTS (Wang et al., 2017), ECSSD (Yan et al., 2013) and SOD (Movahedi and Elder, 2010).

The majority of images across these datasets only contain one single salient object. Scenes including multiple salient objects do exist in each dataset, but the frequency varies from a minimum of 9.8% for ECSSD to 50.3% for HKU-IS, with an average across the datasets of 28%. Of these multi-object images, the majority contain only two objects.

In order to directly evaluate different state-of-the-art SOD models' ability on the multiple salient object detection (MSOD) task, we curate a new dataset, MSOD, containing the most challenging multi-object scenes across the five datasets. To evaluate our, and other methods on complex multi-object images, scenes were only included if they contained three or more salient objects. The total MSOD dataset comprises 300 test images with 1342 total objects. The number of objects in each image varies from 3 to 19 and the distribution is shown in Fig. 6. The dataset comprises a variety of object classes, and a varied number of these objects across the image. We observed that the objects did not exhibit any particular predictable spatial locations.

4.2. Evaluation metrics

Three widely used metrics are applied for performance evaluation: F-measure, mean absolute error (MAE) and the structure-based metric S-measure (Fan et al., 2017). F-measure is a weighted harmonic mean of precision and recall, defined as:

$$F_\beta = \frac{(1+\beta^2) \times Precision \times Recall}{\beta^2 \times Precision + Recall} \quad (15)$$

where β^2 is commonly set to 0.3 in previous works to emphasize precision. Following most state-of-the-art SOD approaches, we report the maximum F_β from all pairs of precision and recall on different thresholds. We also use MAE to compare the prediction map P and ground truth Y, of size $W \times H$, defined as:

$$MAE = \frac{1}{W \times H} \sum_{i=1}^{W} \sum_{j=1}^{H} |P(i,j) - Y(i,j)| \quad (16)$$

Finally, we use S-measure to consider both the region-aware S_r and object-aware S_o structural similarity, defined as:

$$S = \alpha \times S_0 + (1-\alpha) \times S_r \quad (17)$$

where α is set to 0.5 by default. More details about S-measure can be found in Fan et al. (2017).

4.3. Implementation details

The proposed approach is implemented in PyTorch and trained on the DUTS-TR (Wang et al., 2017) dataset, where the salient edge ground truth is calculated by sober operator. To compare our method against other state-of-the-art methods, we train our model using both VGG (Simonyan and Zisserman, 2014) and Resnet-50 (He et al., 2016) backbones. The parameters of backbones are initialized using pretrained models on ImageNet (Krizhevsky et al., 2012), while the weights of newly added layers are initialized randomly. We use the Adam (Kingma and Ba, 2014) optimizer with an initial learning rate of 2e−5, which is divided by 10 after 30 epochs. Our model is trained for 40 epochs in total, which typically takes 3 days in a single 2080Ti with a forward pass taking 0.02 s.

4.4. Comparisons with the state-of-the-art

We compare our proposed method against 14 recent state-of-the-art methods: DSS (Hou et al., 2017), BDMP (Zhang et al., 2018a), PAGR (Zhang et al., 2018b), PiCANet (Liu et al., 2018), RAS (Chen et al., 2018), BASNet (Qin et al., 2019), AFNet (Feng et al., 2019), PoolNet (Liu et al., 2019), EGNet (Zhao et al., 2019), CPD (Wu et al., 2019a), SCRN (Wu et al., 2019b), GateNet (Zhao et al., 2020), MINet (Pang et al., 2020) and SCWSSOD (Yu et al., 2021). For fair comparison, all the saliency maps of competing methods were produced by either pre-trained models, or pre-generated by the authors.

4.4.1. Quantitative comparison

Table 1 shows that our proposed method achieves the best result under 3 evaluation metrics across the datasets. Against the current top approaches: MINet (Pang et al., 2020), PoolNet (Liu et al., 2019), EGNet (Zhao et al., 2019) and SCRN (Wu et al., 2019b), the average improvement of our proposed method on 5 widely used datasets is 0.92%, 2.27%, 2.43% and 4.09% respectively. A further performance improvement can be observed in MSOD dataset, with the average improvement over these approaches increasing to 4.08%, 2.64%, 3.63% and 8.21% respectively. This demonstrates the strong multiple salient object detection ability of our proposed method, which obtains state-of-the-art performance on this challenging dataset.

4.4.2. Precision–recall curves

We plot precision–recall curves over 3 popular SOD datasets and the proposed MSOD dataset in Fig. 7. Our proposed method outperforms all other approaches at most thresholds, especially in the two largest datasets DUT-OMRON and DUTS-TE.

4.4.3. Visual comparison

Qualitative results of our method can be seen in Fig. 8, where our method provides excellent performance in multi-saliency images. Our use of non-local features and top-down feature fusion can make full use of the long-range dependencies between salient objects, with information shared between separate regions of the image.

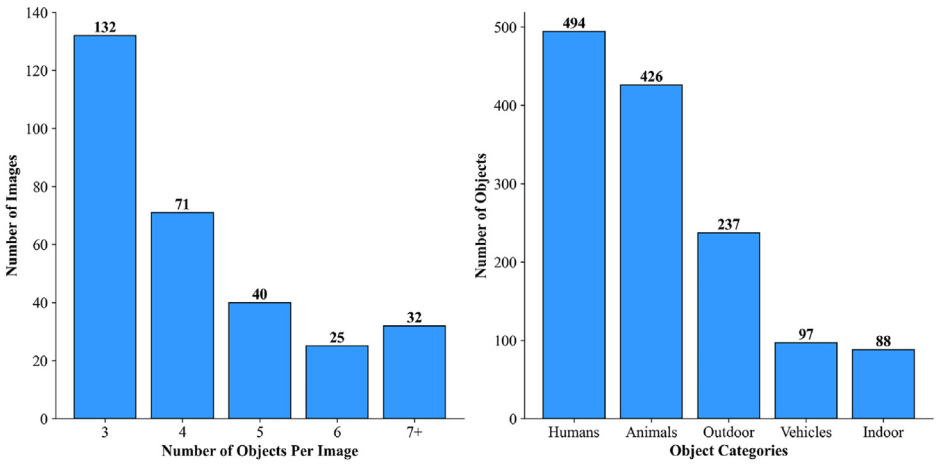

Fig. 6. The distribution of the proposed MSOD dataset. All the images in MSOD dataset contain three or more salient objects to better evaluate the performance of different SOD models in dealing with the multiple salient object detection problem. The dataset contains a variety of object classes, with humans and animals being the most frequent, followed by outdoor scenes and vehicles.

Table 1
Quantitative comparison with other state-of-the-art methods on 5 widely used datasets and the proposed MSOD dataset. ↑ and ↓ indicate higher or lower is better respectively. The best three results among both backbones are marked as **red**, **blue** and **cyan**. Our method achieves top results under 3 evaluation metrics across all datasets without any pre-processing and post-processing.

Model	ECSSD 1000 images			DUTS-TE 5019 images			HKU-IS 1447 images			DUT-O 5168 images			SOD 300 images			MSOD 300 images		
	MaxF ↑	MAE ↓	S ↑	MaxF ↑	MAE ↓	S ↑	MaxF ↑	MAE ↓	S ↑	MaxF ↑	MAE ↓	S ↑	MaxF ↑	MAE ↓	S ↑	MaxF ↑	MAE ↓	S ↑
VGG-Backbone																		
DSS (CVPR2017)	.9207	.0517	.8821	.8251	.0565	.8237	.9161	.0401	.8783	.7812	.0628	.7899	.8410	.1201	.7478	.8240	.0550	.7806
BDMP (CVPR2018)	.9284	.0446	.9109	.8514	.0490	.8616	.9205	.0389	.9065	.7739	.0636	.8091	.8517	.1057	.7833	.8401	.0538	.8379
PAGR (CVPR2018)	.9259	.0608	.8883	.8540	.0555	.8383	.9187	.0475	.8891	.7706	.0709	.7751	.8358	.1447	.7137	.8204	.0627	.7852
RAS (ECCV2018)	.9211	.0564	.8928	.8311	.0594	.8385	.9128	.0454	.8874	.7864	.0617	.8141	.8473	.1225	.7608	.8370	.0597	.8167
BASNet (CVPR2019)	.9425	.0370	.9162	.8594	.0476	.8656	.9297	.0329	.9077	.8052	.0565	.8361	.8487	.1119	.7660	.8396	.0541	.8306
AFNet (CVPR2019)	.9350	.0418	.9134	.8628	.0458	.8666	.9252	.0355	.9058	.7970	.0573	.8258	.8499	.1087	.7700	.8276	.0547	.8191
Ours	.9485	.0344	.9261	**.8894**	.0381	**.8878**	.9350	.0300	.9167	**.8194**	.0541	**.8421**	**.8761**	.0996	.7922	.8531	.0478	.8410
ResNet-Backbone																		
PiCANet (CVPR2018)	.9349	.0464	.9170	.8597	.0506	.8686	.9193	.0437	.9045	.8027	.0653	.8318	.8528	.1024	.7871	.8190	.0641	.8223
PoolNet (CVPR2019)	.9489	.0350	.9263	.8891	**.0368**	.8865	**.9358**	.0300	.9187	.8048	.0539	.8309	.8706	.1034	.7854	.8546	**.0459**	.8429
EGNet (ICCV2019)	.9474	.0374	.9247	.8885	.0392	.8868	.9352	.0309	.9179	.8152	**.0531**	.8408	**.8778**	.0969	**.8000**	.8516	.0470	.8402
CPD (CVPR2019)	.9393	.0371	.9181	.8653	.0434	.8689	.9252	.0339	.9064	.7964	.0560	.8247	.8568	.1095	.7646	.8241	.0539	.8109
SCRN (ICCV2019)	**.9496**	.0375	**.9272**	.8875	.0398	.8847	.9351	.0332	.9169	.8112	.0560	.8364	.8655	.1046	.7851	.8384	.0527	.8244
GateNet (ECCV2020)	.9454	.0401	.9198	.8873	.0401	.8847	.9334	.0331	.9153	.8178	.0549	.8380	.8731	.0981	.7948	**.8623**	.0483	**.8507**
MINet (CVPR2020)	.9475	**.0335**	.9249	.8836	.0372	.8837	.9353	**.0283**	**.9197**	.8097	.0555	.8325	.8730	**.0905**	.7973	.8472	.0474	.8400
SCWSSOD[a] (AAAI2021)	.9145	.0489	.8818	.8440	.0487	.8405	.9111	.0375	.8824	.7823	.0602	.8117	.8367	.1077	.7503	.8329	.0534	.8060
Ours	**.9519**	**.0325**	**.9297**	**.8967**	**.0358**	**.8946**	**.9389**	**.0293**	**.9218**	**.8234**	**.0530**	**.8470**	**.8786**	**.0934**	**.8024**	**.8720**	**.0442**	**.8614**

[a]Denotes weakly-supervised methods

4.5. Ablation studies

In this section we investigate the contribution of different components in our proposed approach. All experiments are based on VGG backbone and two largest datasets: DUTS-TE and DUT-OMRON.

4.5.1. Effectiveness of NLGM

Compared to a baseline structure (1st row in Table 2), non-local guidance (2nd row) provides performance gains across all evaluation metrics on both datasets. This demonstrates the effectiveness of capturing long-range dependencies in NLGM.

4.5.2. Effectiveness of FFG

Incorporating feature fusion (the 4th and 6th row in Table 2) can also improve the performance beyond the ones without FFG across all metrics on both datasets, indicating the importance of filtering the redundant information from each part of the architecture.

Table 2
Ablation analysis of different components in our proposed architecture.

Models				DUTS-TE			DUT-OMRON		
NLGM	FFG	ERM	E	MaxF ↑	MAE ↓	S ↑	MaxF ↑	MAE ↓	S ↑
				.8761	.0425	.8750	.7958	.0575	.8276
✓				.8836	.0410	.8809	.8103	.0562	.8357
✓		✓		.8847	.0410	.8839	.8138	.0563	.8366
✓	✓			.8858	.0396	.8857	.8153	.0560	.8379
✓	✓		✓	.8882	.0395	.8862	.8175	.0543	.8407
✓	✓	✓		**.8894**	**.0381**	**.8878**	**.8194**	**.0541**	**.8421**

4.5.3. Effectiveness of ERM

As shown in Table 2, E denotes just the output of the first ERB layer, which is then passed into different stages of our decoder in a mechanism similar to the approach used in EGNet (Zhao et al., 2019). By introducing ERM, we see an improvement in performance (5th row and 6th row in Table 2). We hypothesize that the convolution operations of ERM, applied in a cascade manner, help edge features

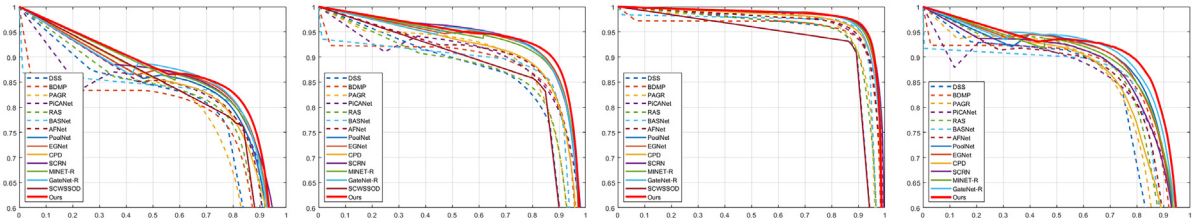

(a) DUT-OMRON (b) DUTS-TE (c) ECSSD (d) MSOD

Fig. 7. Precision (vertical axis) recall (horizontal axis) curves on three popular salient object detection datasets and the proposed MSOD dataset. The red solid line demonstrates our proposed method. (For interpretation of the references to color in this figure legend, the reader is referred to the web version of this article.)

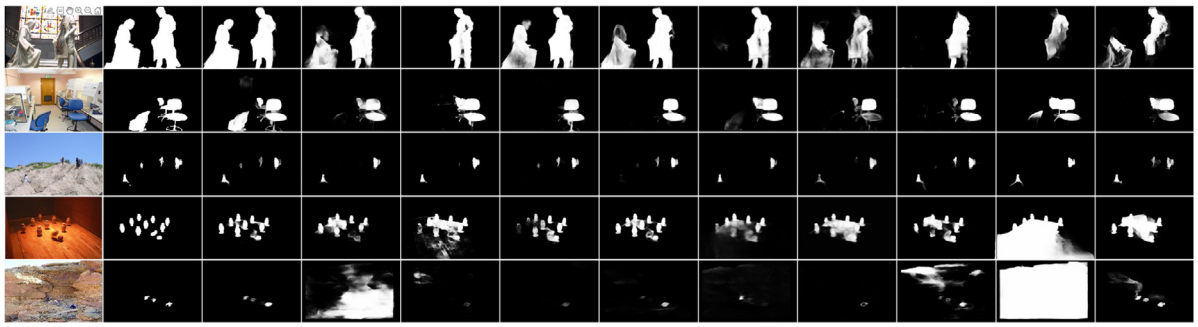

Fig. 8. Qualitative comparisons with state-of-the-art approaches over some of the challenging images.

Table 3
Performance comparison of different NLGM configurations. SSNLB and CSNLB refer to spatial-space non-local block and channel-space non-local block respectively. All three configurations are without FFG and ERM.

NLGM Configurations	DUTS-TE			DUT-OMRON		
	MaxF ↑	MAE ↓	S ↑	MaxF ↑	MAE ↓	S ↑
SSNLB	.8813	.0411	.8789	.8081	.0563	.8336
CSNLB	.8816	.0415	.8790	.8079	.0566	.8348
SSNLB+CSNLB	**.8836**	**.0410**	**.8809**	**.8103**	**.0562**	**.8357**

Table 4
Performance comparison of different NLGM architectures. All structures here are without FFG and ERM.

NLGM Architectures	DUTS-TE			DUT-OMRON		
	MaxF ↑	MAE ↓	S ↑	MaxF ↑	MAE ↓	S ↑
(a)	.8796	.0419	.8787	.8052	.0567	.8313
(b)	.8815	.0415	.8801	.8075	.0565	.8330
(c)	.8816	.0417	.8805	.8083	.0565	.8345
(d)	**.8836**	**.0410**	**.8809**	**.8103**	**.0562**	**.8357**

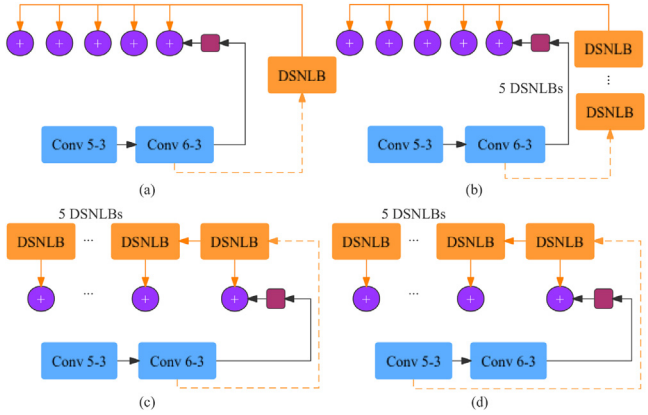

Fig. 9. Different architectures of NLGM. All structures here are without FFG and ERGM. Element-wise addition operation is used at each stage to fuse different features.

to adaptively support the training of non-local and salient features in different stages/resolutions.

4.5.4. Effectiveness of NLGM & ERM

Compared to 2nd row, the 3rd row in Table 2 has a higher performance, which proves the effectiveness of introducing both NLGM and ERM. Features that are mutually beneficial to both non-local and edge saliency are emphasized. These modules appear to complement each other, with non-local, edge and saliency all contributing to the accurate recovery of salient regions.

4.5.5. Effectiveness of FFG & ERM

By introducing edge features as part of the FFG, performance gains can be observed (6th row and 4th row in Table 2), which demonstrates that the edge refinement module effectively promotes relevant salient features prior to their combination within the FFG.

4.5.6. Configurations of NLGM

As shown in Table 3, we conduct experiments to investigate the performance of different configurations of NLGM. Compared to the baseline (1st row in Table 2), the models incorporating SSNLB (1st row in Table 3) or CSNLB (2nd row in Table 3) both improve performance on two datasets. The best performance is obtained when using both SSNLB and CSNLB together (3rd row in Table 3), showing that these two modules are highly complimentary, and that both spatial and channel-wise non-local features contribute to image saliency.

4.5.7. Architectures of NLGM

We perform experiments to explore the effect of different structures of NLGM. We evaluate four different architectures to incorporate non-local information into our U-shape network. The architectures and the corresponding performance are shown in Fig. 9 and Table 4. Our baseline model (a) utilizes a single DSNLB drawing features from S^6, with the same output distributed to all top-down stages. Model (b) incorporates a stack of 5 DSNLBs in this same construction, evaluating

the effect of chains of non-local blocks over single instances. We find that a stack of DSNLBs improve performance on all metrics, indicating the effectiveness of long-range multi-hop communications that build richer relevant salient features across both spatial and channel space. Model (c) draws features again from S^6 but distributes the DSNLBs throughout the top-down pathway as per our main architecture in Fig. 2. Performance is again improved a little, likely because this one-to-one guidance method can generate adaptive non-local features appropriate to each scale of saliency features F. Finally, model (d) draws features from S^5 as our final architecture does. The improvement suggests that the increased spatial size of these features is better exploited by the DSNLBs over the relatively small spatial size of that in S^6.

5. Conclusion

In this paper we seek to address the problem of segmenting multiple salient objects in complex scenes. We present a new architecture for salient object detection, utilizing both spatial and channel-wise long-range dependencies. A non-local guidance module captures long-range dependencies between salient objects across the image, allowing the network to better resolve multiple separate salient objects. We also design a feature fusion gate that combines salient and non-local features. The gate utilizes progressively refined edge features to promote the most relevant features drawn from each module. Our approach shows state-of-the-art performance across 5 widely used salient object datasets. We also curate an additional dataset comprising only multiple objects in challenging scenes, and show that the performance gap between ours and other methods widens. Consideration of complex scenes is required to further drive development in image saliency, our network and the new dataset can be used as a baseline for performance in this domain.

CRediT authorship contribution statement

Bowen Deng: Methodology, Software, Data curation, Writing – original draft. **Andrew P. French:** Supervision, Writing – review & editing. **Michael P. Pound:** Supervision, Conceptualisation, Writing – review & editing.

Declaration of competing interest

The authors declare that they have no known competing financial interests or personal relationships that could have appeared to influence the work reported in this paper.

Data availability

Data will be made available on request.

Acknowledgments

This work was funded by the University of Nottingham's Future Food Beacon, and the Biotechnology and Biological Sciences Research Council grant BB/T012129/1.

References

Borji, A., Cheng, M.-M., Hou, Q., Jiang, H., Li, J., 2019. Salient object detection: A survey. Comput. Vis. Media 1–34.

Chen, S., Tan, X., Wang, B., Hu, X., 2018. Reverse attention for salient object detection. In: Proceedings of the European Conference on Computer Vision. ECCV, pp. 234–250.

Cheng, M.-M., Mitra, N.J., Huang, X., Torr, P.H., Hu, S.-M., 2014. Global contrast based salient region detection. IEEE Trans. Pattern Anal. Mach. Intell. 37 (3), 569–582.

Das, A., Agrawal, H., Zitnick, L., Parikh, D., Batra, D., 2017. Human attention in visual question answering: Do humans and deep networks look at the same regions? Comput. Vis. Image Underst. 163, 90–100.

Fan, D.-P., Cheng, M.-M., Liu, Y., Li, T., Borji, A., 2017. Structure-measure: A new way to evaluate foreground maps. In: Proceedings of the IEEE International Conference on Computer Vision. pp. 4548–4557.

Fang, H., Gupta, S., Iandola, F., Srivastava, R.K., Deng, L., Dollár, P., Gao, J., He, X., Mitchell, M., Platt, J.C., et al., 2015. From captions to visual concepts and back. In: Proceedings of the IEEE Conference on Computer Vision and Pattern Recognition. pp. 1473–1482.

Feng, M., Lu, H., Ding, E., 2019. Attentive feedback network for boundary-aware salient object detection. In: Proceedings of the IEEE Conference on Computer Vision and Pattern Recognition. pp. 1623–1632.

Fu, J., Liu, J., Tian, H., Li, Y., Bao, Y., Fang, Z., Lu, H., 2019. Dual attention network for scene segmentation. In: Proceedings of the IEEE Conference on Computer Vision and Pattern Recognition. pp. 3146–3154.

He, J., Feng, J., Liu, X., Cheng, T., Lin, T.-H., Chung, H., Chang, S.-F., 2012. Mobile product search with bag of hash bits and boundary reranking. In: 2012 IEEE Conference on Computer Vision and Pattern Recognition. IEEE, pp. 3005–3012.

He, K., Zhang, X., Ren, S., Sun, J., 2016. Deep residual learning for image recognition. In: Proceedings of the IEEE Conference on Computer Vision and Pattern Recognition. pp. 770–778.

Hou, Q., Cheng, M.-M., Hu, X., Borji, A., Tu, Z., Torr, P.H., 2017. Deeply supervised salient object detection with short connections. In: Proceedings of the IEEE Conference on Computer Vision and Pattern Recognition. pp. 3203–3212.

Hou, Q., Cheng, M., Hu, X., Borji, A., Tu, Z., Torr, P., 2019. Deeply supervised salient object detection with short connections. IEEE Trans. Pattern Anal. Mach. Intell. 41 (4).

Jiang, H., Wang, J., Yuan, Z., Wu, Y., Zheng, N., Li, S., 2013. Salient object detection: A discriminative regional feature integration approach. In: Proceedings of the IEEE Conference on Computer Vision and Pattern Recognition. pp. 2083–2090.

Kingma, D.P., Ba, J., 2014. Adam: A method for stochastic optimization. arXiv preprint arXiv:1412.6980.

Krizhevsky, A., Sutskever, I., Hinton, G.E., 2012. Imagenet classification with deep convolutional neural networks. In: Advances in Neural Information Processing Systems. pp. 1097–1105.

Lee, C.-Y., Xie, S., Gallagher, P., Zhang, Z., Tu, Z., 2015. Deeply-supervised nets. In: Artificial Intelligence and Statistics. pp. 562–570.

Li, A., Qi, J., Lu, H., 2020. Multi-attention guided feature fusion network for salient object detection. Neurocomputing 411, 416–427.

Li, G., Yu, Y., 2015. Visual saliency based on multiscale deep features. In: Proceedings of the IEEE Conference on Computer Vision and Pattern Recognition. pp. 5455–5463.

Liu, N., Han, J., Yang, M.-H., 2018. Picanet: Learning pixel-wise contextual attention for saliency detection. In: Proceedings of the IEEE Conference on Computer Vision and Pattern Recognition. pp. 3089–3098.

Liu, J.-J., Hou, Q., Cheng, M.-M., Feng, J., Jiang, J., 2019. A simple pooling-based design for real-time salient object detection. In: Proceedings of the IEEE Conference on Computer Vision and Pattern Recognition. pp. 3917–3926.

Liu, N., Zhang, N., Han, J., 2020. Learning selective self-mutual attention for RGB-D saliency detection. In: Proceedings of the IEEE/CVF Conference on Computer Vision and Pattern Recognition. pp. 13756–13765.

Long, J., Shelhamer, E., Darrell, T., 2015. Fully convolutional networks for semantic segmentation. In: Proceedings of the IEEE Conference on Computer Vision and Pattern Recognition. pp. 3431–3440.

Movahedi, V., Elder, J.H., 2010. Design and perceptual validation of performance measures for salient object segmentation. In: 2010 IEEE Computer Society Conference on Computer Vision and Pattern Recognition-Workshops. IEEE, pp. 49–56.

Pang, Y., Zhao, X., Zhang, L., Lu, H., 2020. Multi-scale interactive network for salient object detection. In: Proceedings of the IEEE/CVF Conference on Computer Vision and Pattern Recognition. pp. 9413–9422.

Peng, C., Zhang, X., Yu, G., Luo, G., Sun, J., 2017. Large kernel matters–improve semantic segmentation by global convolutional network. In: Proceedings of the IEEE Conference on Computer Vision and Pattern Recognition. pp. 4353–4361.

Qin, X., Zhang, Z., Huang, C., Gao, C., Dehghan, M., Jagersand, M., 2019. Basnet: Boundary-aware salient object detection. In: Proceedings of the IEEE Conference on Computer Vision and Pattern Recognition. pp. 7479–7489.

Ren, Z., Gao, S., Chia, L.-T., Tsang, I.W.-H., 2013. Region-based saliency detection and its application in object recognition. IEEE Trans. Circuits Syst. Video Technol. 24 (5), 769–779.

Ronneberger, O., Fischer, P., Brox, T., 2015. U-net: Convolutional networks for biomedical image segmentation. In: International Conference on Medical Image Computing and Computer-Assisted Intervention. Springer, pp. 234–241.

Rutishauser, U., Walther, D., Koch, C., Perona, P., 2004. Is bottom-up attention useful for object recognition? In: Proceedings of the 2004 IEEE Computer Society Conference on Computer Vision and Pattern Recognition, 2004. CVPR 2004. Vol. 2. IEEE, p. II.

Simonyan, K., Zisserman, A., 2014. Very deep convolutional networks for large-scale image recognition. arXiv preprint arXiv:1409.1556.

Sun, F., Li, W., Guan, Y., 2019. Self-attention recurrent network for saliency detection. Multimedia Tools Appl. 78 (21), 30793–30807.

Wang, X., Girshick, R., Gupta, A., He, K., 2018b. Non-local neural networks. In: Proceedings of the IEEE Conference on Computer Vision and Pattern Recognition. pp. 7794–7803.

Wang, L., Lu, H., Ruan, X., Yang, M.-H., 2015. Deep networks for saliency detection via local estimation and global search. In: Proceedings of the IEEE Conference on Computer Vision and Pattern Recognition. pp. 3183–3192.

Wang, L., Lu, H., Wang, Y., Feng, M., Wang, D., Yin, B., Ruan, X., 2017. Learning to detect salient objects with image-level supervision. In: Proceedings of the IEEE Conference on Computer Vision and Pattern Recognition. pp. 136–145.

Wang, W., Shen, J., Ling, H., 2018a. A deep network solution for attention and aesthetics aware photo cropping. IEEE Trans. Pattern Anal. Mach. Intell. 41 (7), 1531–1544.

Wang, X., You, S., Li, X., Ma, H., 2018c. Weakly-supervised semantic segmentation by iteratively mining common object features. In: Proceedings of the IEEE Conference on Computer Vision and Pattern Recognition. pp. 1354–1362.

Wei, Y., Liang, X., Chen, Y., Shen, X., Cheng, M.-M., Feng, J., Zhao, Y., Yan, S., 2016. Stc: A simple to complex framework for weakly-supervised semantic segmentation. IEEE Trans. Pattern Anal. Mach. Intell. 39 (11), 2314–2320.

Wei, Y., Wen, F., Zhu, W., Sun, J., 2012. Geodesic saliency using background priors. In: European Conference on Computer Vision. Springer, pp. 29–42.

Wu, Z., Su, L., Huang, Q., 2019a. Cascaded partial decoder for fast and accurate salient object detection. In: Proceedings of the IEEE Conference on Computer Vision and Pattern Recognition. pp. 3907–3916.

Wu, Z., Su, L., Huang, Q., 2019b. Stacked cross refinement network for edge-aware salient object detection. In: Proceedings of the IEEE International Conference on Computer Vision. pp. 7264–7273.

Yan, Q., Xu, L., Shi, J., Jia, J., 2013. Hierarchical saliency detection. In: Proceedings of the IEEE Conference on Computer Vision and Pattern Recognition. pp. 1155–1162.

Yang, C., Zhang, L., Lu, H., Ruan, X., Yang, M.-H., 2013. Saliency detection via graph-based manifold ranking. In: Proceedings of the IEEE Conference on Computer Vision and Pattern Recognition. pp. 3166–3173.

Yu, S., Zhang, B., Xiao, J., Lim, E.G., 2021. Structure-consistent weakly supervised salient object detection with local saliency coherence. In: Proceedings of the AAAI Conference on Artificial Intelligence. AAAI.

Zhang, L., Dai, J., Lu, H., He, Y., Wang, G., 2018a. A bi-directional message passing model for salient object detection. In: Proceedings of the IEEE Conference on Computer Vision and Pattern Recognition. pp. 1741–1750.

Zhang, D., Meng, D., Zhao, L., Han, J., 2017. Bridging saliency detection to weakly supervised object detection based on self-paced curriculum learning. arXiv preprint arXiv:1703.01290.

Zhang, X., Wang, T., Qi, J., Lu, H., Wang, G., 2018b. Progressive attention guided recurrent network for salient object detection. In: Proceedings of the IEEE Conference on Computer Vision and Pattern Recognition. pp. 714–722.

Zhao, J.-X., Liu, J.-J., Fan, D.-P., Cao, Y., Yang, J., Cheng, M.-M., 2019. Egnet: Edge guidance network for salient object detection. In: Proceedings of the IEEE International Conference on Computer Vision. pp. 8779–8788.

Zhao, R., Ouyang, W., Li, H., Wang, X., 2015. Saliency detection by multi-context deep learning. In: Proceedings of the IEEE Conference on Computer Vision and Pattern Recognition. pp. 1265–1274.

Zhao, X., Pang, Y., Zhang, L., Lu, H., Zhang, L., 2020. Suppress and balance: A simple gated network for salient object detection. In: European Conference on Computer Vision. Springer, pp. 35–51.

Zhao, H., Shi, J., Qi, X., Wang, X., Jia, J., 2017. Pyramid scene parsing network. In: Proceedings of the IEEE Conference on Computer Vision and Pattern Recognition. pp. 2881–2890.

Zhou, Z., Wang, Z., Lu, H., Wang, S., Sun, M., 2020. Multi-type self-attention guided degraded saliency detection.. In: AAAI. pp. 13082–13089.

Zhu, W., Liang, S., Wei, Y., Sun, J., 2014. Saliency optimization from robust background detection. In: Proceedings of the IEEE Conference on Computer Vision and Pattern Recognition. pp. 2814–2821.